

Prediction of Interfacial Properties of High-Performance Polymers and Flattened CNT-Reinforced Composites using Molecular Dynamics

*Prathamesh P. Deshpande, Matthew S. Radue, Prashik Gaikwad, Swapnil Bamane, Sagar Umesh Patil,
William A. Pisani, Gregory M. Odegard**

Michigan Technological University, Houghton, MI-49931

Keywords

Computational Materials, Molecular Dynamics, Interface/interphase, High-performance polymer composites

Abstract

The next generation of ultra-high strength composites for structural components of vehicles for manned missions to deep space will likely incorporate flattened carbon nanotubes (flCNTs). With a wide range of

* Corresponding Author.

Email address: gmodegar@mtu.edu (Gregory M. Odegard)

high-performance polymers to choose from as the matrix component, efficient and accurate computational modeling can be used to efficiently down-select compatible resins, drive the design of these composites by predicting interface behavior, and provide critical physical insight into the fCNT/polymer interface. In this study, molecular dynamics simulation is used to predict the interaction energy, frictional sliding resistance, and mechanical binding of fCNT/polymer interfaces for epoxy, bismaleimide (BMI), and benzoxazine high-performance resins. The results indicate that the BMI has stronger interfacial interaction and transverse tension binding with fCNT interfaces, while the benzoxazine demonstrates the strongest levels of interfacial friction resistance. Comparison of these results with similar results from the literature for other high-performance resins indicates that BMI demonstrates the best overall compatibility with fCNTs for use in high-performance structural composites.

Introduction

The need for lightweight ultra-strong structural materials is increasingly being recognized for the next generation of space vehicles for deep-space human travel. To fulfill this need, significant focus has been placed on carbon nanotube (CNT) based composites materials [1-4]. These materials have the potential to exhibit superior thermo-mechanical properties relative to the current state-of-the-art composites [5, 6]. So far, a major shortcoming of these materials is their failure to translate these outstanding properties to higher length scales. Therefore, it is necessary to investigate and mitigate the failure of the CNT/matrix interfacial region to fully utilize the benefits of these materials.

A recent study by Downes et al. [7] introduced a novel fabrication method which generates stacks of flattened CNTs (fCNTs) resulting in self-aligned assemblages. These structures promote higher surface-to-surface contact which was evident when combined with a bismaleimide polymer matrix. The fCNT/BMI composite showed a twofold increase in tensile strength and a threefold increase in the tensile

modulus when compared to the round CNT composite counterpart [7]. Even though the fCNT-fCNT contact was enhanced by the flattening and stacking, the TEM-observed fracture surfaces showed intra-stack sliding in addition to complete stack pullout. A follow-up study by Jolowsky et al. [8] provided a pathway to scale the fCNT composite fabrication method to macro-scale panels with excellent mechanical properties.

Although these early experimental studies showed promising results for the development of fCNT composites, they did not address the influence of different resin types on the panel-level mechanical performance. Many studies have addressed the interfacial characteristics of CNT/polymer composites [9, 10], however, none of these studies provide a comprehensive view of the influence of resin type on composite performance, and none of them address fCNT/polymer interfaces directly. Indeed, such studies for a large range of resin types are difficult to achieve experimentally because of the difficulty and expense of fabricating and testing fCNT composites. Computational approaches are needed to efficiently drive the development and design of future fCNT composites.

Patil et al. [11] reported the polymer/fCNT interfacial characteristics for two polyimide systems at the nanoscale using Molecular Dynamics (MD) techniques. It was reported that different chemical groups in the polymer had different effects on the polymer/fCNT interfacial interaction. Findings by Pisani et al. [12] affirmed the same by comparing PEEK and fluorinated and non-fluorinated cyanate esters.

Using MD, this study focuses on modelling the polymer/fCNT interface of three high-performance polymers: glycidylamine-based epoxy, bismaleimide (BMI), and poly-benzoxazine. All the simulated systems are aerospace-relevant thermosets [13-21] and each system is unique in terms of reaction chemistry and molecular topology. This study compliments the results published by Patil et al. [11] and Pisani et al. [12].

It is important to note that similar to Patil et al. [11] and Pisani et al. [12], experimental validation of the simulated results is not performed because fabrication and the relevant interfacial characterization methods for these materials have not yet been developed. That is, it is not yet possible to consistently fabricate fCNT/polymer nanocomposites with perfect, uniform resin infusion throughout the bulk composite. Even if such fabrication was currently possible, computational simulation can still provide physical insight that experimental characterization methods cannot. Therefore, this study is intended to drive the future development of such materials in a consistent, efficient manner. The simulations discussed herein employ MD modelling techniques which have been previously experimentally validated [22-24].

Molecular Modeling

The details of the MD simulation are discussed in this section. The LAMMPS software package was used for all simulations discussed in this paper [25]. The Interface Force Field (IFF), developed by Heinz et al. [26], was designed to accurately model the properties of inorganic surfaces. Included in the original scope of IFF is the ability to capture inorganic-organic interfaces and the adsorption of organic molecules onto inorganic surfaces. Recently, the Polymer Consistent Force Field was supplemented with IFF (PCFF-IFF) and proven successful for predicting the dispersibility of CNTs in different solvents and polymer solutions [27]. The PCFF-IFF forcefield was used to assign the interatomic potential in this study, as it was previously shown to yield accurate results for fCNTs and consists of all the relevant atom types associated with the amorphous polymer systems [11, 28]. Additionally, this force field can model the π electrons virtually which is critical to accurately capture the polymer-fCNT interface. The PCFF-IFF force field is well-known for its accurate atomic charge assignments, which has proven to have a significant effect on the predicted matrix-reinforcement interface characteristics and molecular conformations of polar molecules [11, 12].

Material Systems

The epoxy, BMI, and benzoxazine systems selected for this study consisted of the following monomers:

1. Epoxy: Tetraglycidyl methylenedianiline (TGMDA or TGDDM) and 4,4'-diaminodiphenyl sulfone (DDS) [29]
2. BMI: Bismaleimidodiphenylmethane (BMPM) and O,O'-diallyl bisphenol A (DABPA) [30]
3. Benzoxazine: Bisphenol-A benzoxazine [31]

High-performance polymer-based composite materials are extensively used in aerospace applications because of their excellent thermal and mechanical properties [2, 32]. These three polymer systems are thermosets that are specifically used for structural applications [14, 31, 33-37]. Molecular modeling studies exploring the thermo-mechanical properties have been previously performed on these specific polymers [29, 30, 38-41]. However, the influence of the molecular structure on the overall mechanical properties and reinforcement interface characteristics remains largely unexplored. Figure 1 shows the molecular structures of all the modelled monomers. 1:1 molar ratios of BMPM to DABPA and TGMDA to DDS were used for the BMI and epoxy polymers, respectively [24, 29, 30, 38].

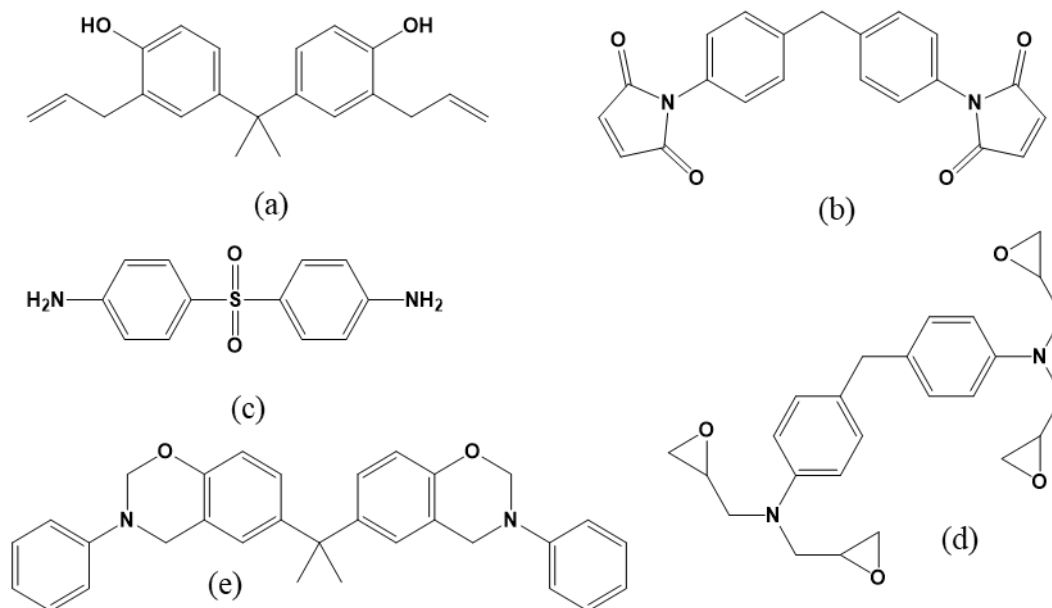


Figure 1. Chemical structures of (a) DABPA, (b) BMPM, (c) DDS, (d) TGMDA, and (e) Benzoxazine.

Model Setup

Figure 2 shows a representative MD model where the two f1CNTs are modeled as two double-layered graphene surfaces, simply representing the flattened portion of the f1CNTs. The rounded ends of the f1CNTs shown in Figure 2(b) were excluded for computational efficiency [11, 12], as these features can be better captured with larger length scale models and this study is only focused on isolating the influence of the resin type on interfacial characteristics in the flattened region.

In this work, previously established methodology has been adopted to model the three thermoset polymer composites using MD [11, 12], and the details are proved in the Supporting Information. All the simulation box boundaries are periodic, hence the polymer regions connected across the top and bottom of the Z boundary make up a single layer. This layered setup was chosen to represent the basic features of the sp^2 carbon f1CNT-polymer interaction, friction, and transverse strength. While the model simulates the ideal scenario of complete polymer resin infiltration between f1CNTs, the described setup is useful in extracting the critical interfacial features in the nanocomposite [42]. It is important to note that MD modeling predictions are generally very sensitive to the modeling parameters. The modeling parameters used herein have been chosen to be consistent with those from previous MD studies [11, 12] to provide objective consistency between the results. Thus, these results are generated for the purpose of comparative studies between different f1CNT/polymer interfaces. The modeling parameters were not chosen to mimic specific experimental conditions, because, as mentioned above, no methods have been developed yet to fabricate such ideally-structured materials.

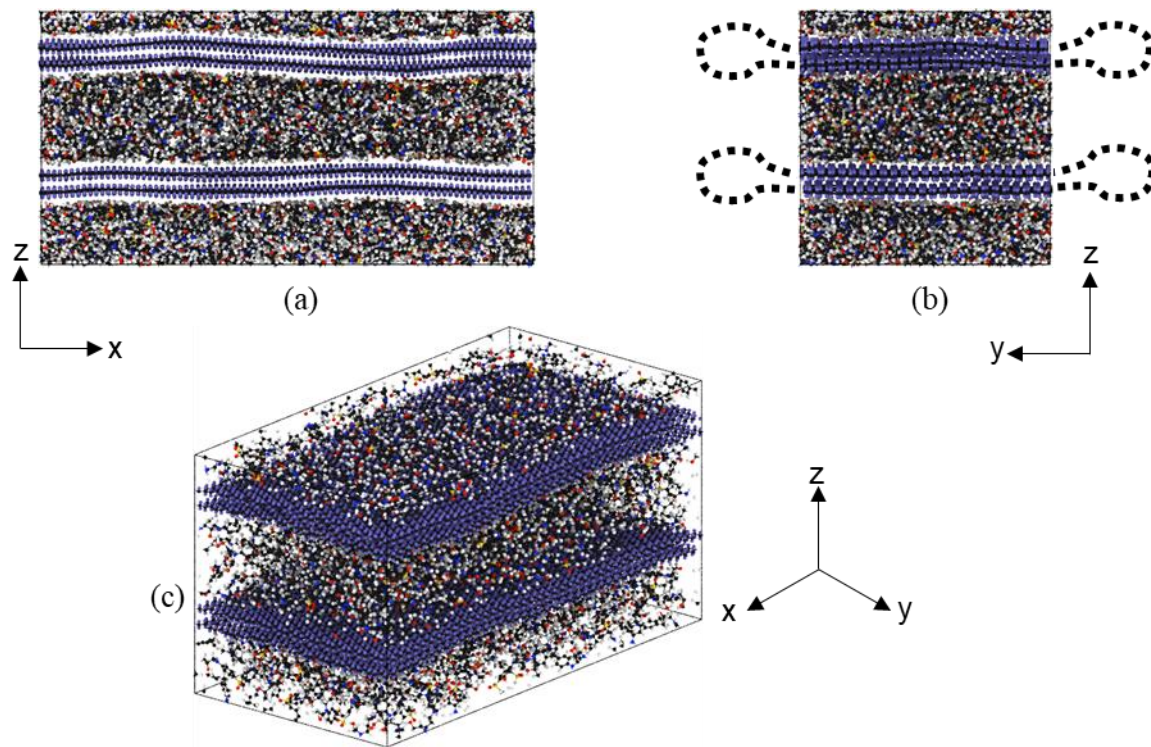


Figure 2. Representative model setup for the flCNT/epoxy composite (a) front view, (b) side view showing the side lobes of flCNTs, and (c) isometric view. The purple atoms attached to the flCNT carbon atoms represent the virtual π electrons.

Error! Reference source not found.5 shows the atomic mass densities along Z-direction and highlights the higher atomic densities near the interface for all the models. The z-direction axis has been normalized, such that the width of the flCNT peaks appears different for each system, even though they have the same structural dimensions. The higher polymer density at the interface can be seen in the form of a secondary peak (red-dotted circles) adjacent to the larger peaks, which represent flCNT atoms. Figure 3 shows the polymerized models for different polymer mass fractions. Within these figures, the left-most image displays the lowest polymer mass fraction resulting in clustering of polymer atoms. The middle image displays a perfectly saturated interface with the two flCNT layers completely separated by the polymer atoms. The right-most image displays the highest polymer mass fraction which results in addition of

excessive polymer atoms. Detailed polymer mass fractions and the respective molecular masses are included in the Supporting Information, Section S3.

The equilibrated models were then evaluated for the interfacial interaction energy, friction resistance, and transverse strength. The interaction energy and friction simulations were also carried out on unpolymerized models to assess the effect of polymerization. To compute the interaction energy, the purely non-bonded potential energy unrelated to the polymer and f1CNTs was extracted from the model using the help of the “compute group/group” command in LAMMPS [43, 44]. For all models, the simulations were performed in the NPT ensemble over 0.5 ns to collect the time-averaged interaction energy data. Temperature and pressure settings of 300 K and 1 atm respectively were used for all of these simulations.

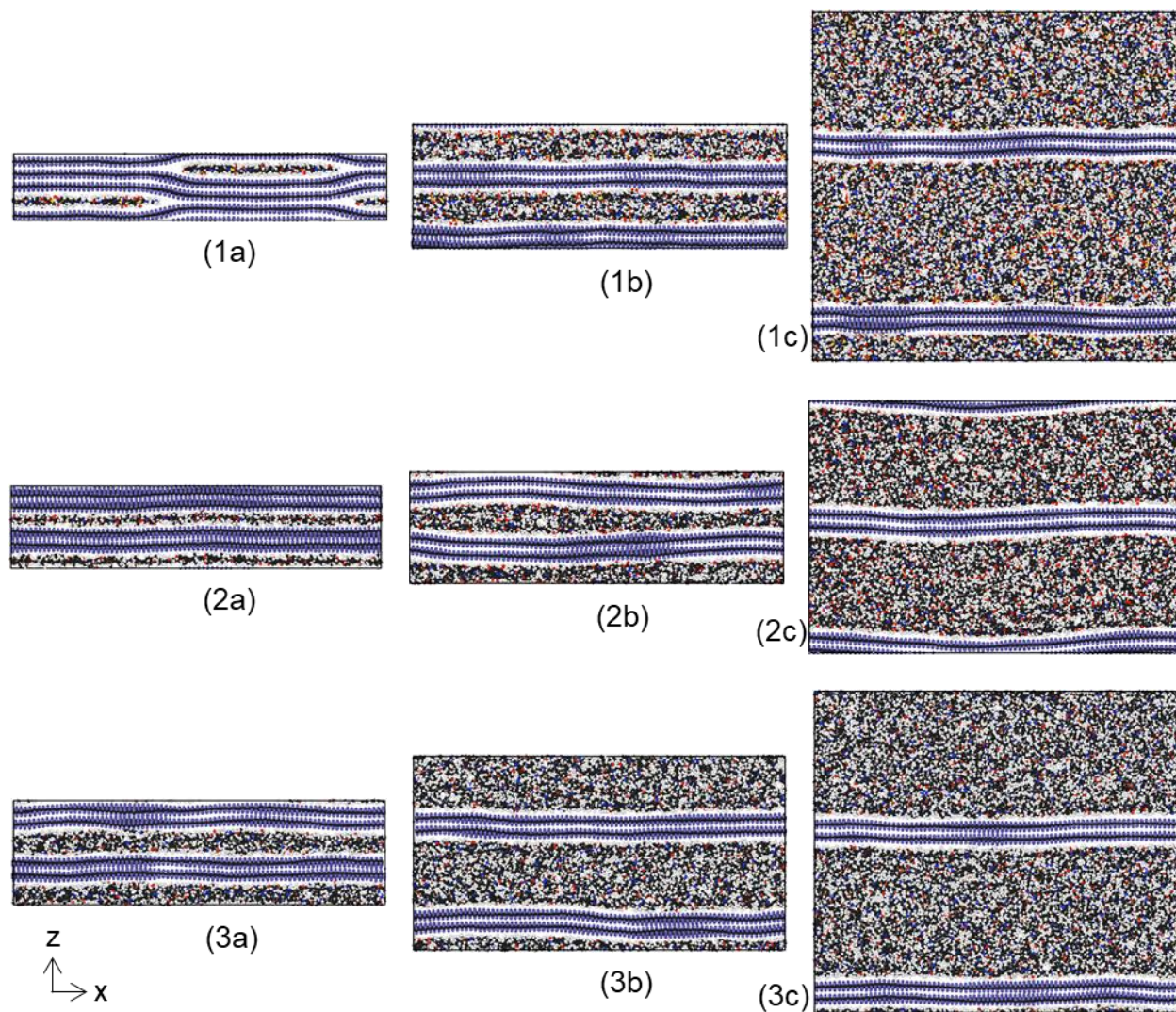


Figure 3. Molecular models of flCNT/epoxy (top), flCNT/BMI (middle), and flCNT/benzoxazine (bottom) composites with mass fraction- (1a) 10%, (1b) 41%, (1c) 75%, (2a) 22% (2b) 36% (2c) 66%, (3a) 20%, (3b) 34%, and (3c) 56%.

Patil et al. [11] demonstrated a novel approach to compute atomistic friction force between polymer-infiltrated flCNTs using the same simulation geometry described herein. Using the same approach, friction simulations were performed on both the unpolymerized and polymerized models for each resin system. For all the models, both the flCNTs (both top and bottom walls of the flCNT layers) were tethered to two distinct points with a virtual spring using LAMMPS. Thus, the walls within a single layer of flCNTs were

not allowed to slide with respect to each other such that the friction between the f1CNT/polymer interface could be isolated. The spring constant used for both the springs was set to 1 kcal/mol·Å². The point connected to the bottom layer was linearly displaced in the X direction using a velocity range of 0.1 Å/ps to 5 Å/ps. The other layer was held in position using the NPT ensemble with 300 K temperature and 1 atm pressure. The polymer layers and the sliding f1CNT were maintained under the NVE ensemble, allowing the temperature to change, and thus enhancing the vibrations at the interfaces. The resulting friction force was computed between the moving f1CNT and the polymer layer, and the fixed f1CNT and the polymer layer.

The third criterion studied is the transverse strength of the layered models. The equilibrated models of the three polymer systems with a polymer mass fraction of approximately 0.4 were used for this evaluation. This polymer mass fraction is comparable with previously reported data [11, 12]. To assess the transverse tension behavior, the simulation box was subjected to a uniaxial strain in the direction perpendicular to the f1CNT plane at a constant strain rate of $2 \times 10^8 \text{ s}^{-1}$ until there was total separation of one of the CNT/polymer interfaces or a maximum of 150% strain was reached. The overall system stresses and strains were recorded, and the corresponding stiffness, strength, and toughness values were calculated [11]. An R script was used for this analysis. It is important to note that in these simulations, the upper and lower walls of single layers of f1CNTs did not separate from each other, as the f1CNT/polymer interface always failed first. Thus, the results are naturally focused only on the f1CNT/polymer interface mechanical behavior.

Results

Interaction energy

The interaction energy for the unpolymerized and polymerized models of the three resins are shown in Figure 4. The displayed trendlines are to distinguish multiple datasets and provide clear trends amongst

the scattered data points. It is important to note that the trendlines do not bear any physical significance. The interaction energy values carry a negative sign which indicates attraction to the aromatic surface of the f1CNT. Therefore, higher negative values indicate greater polymer/surface affinity. Figure 4 shows dramatic increases in interaction energy for all the three systems, both monomer and polymer, with increases in polymer mass fraction, except for the polymerized benzoxazine system.

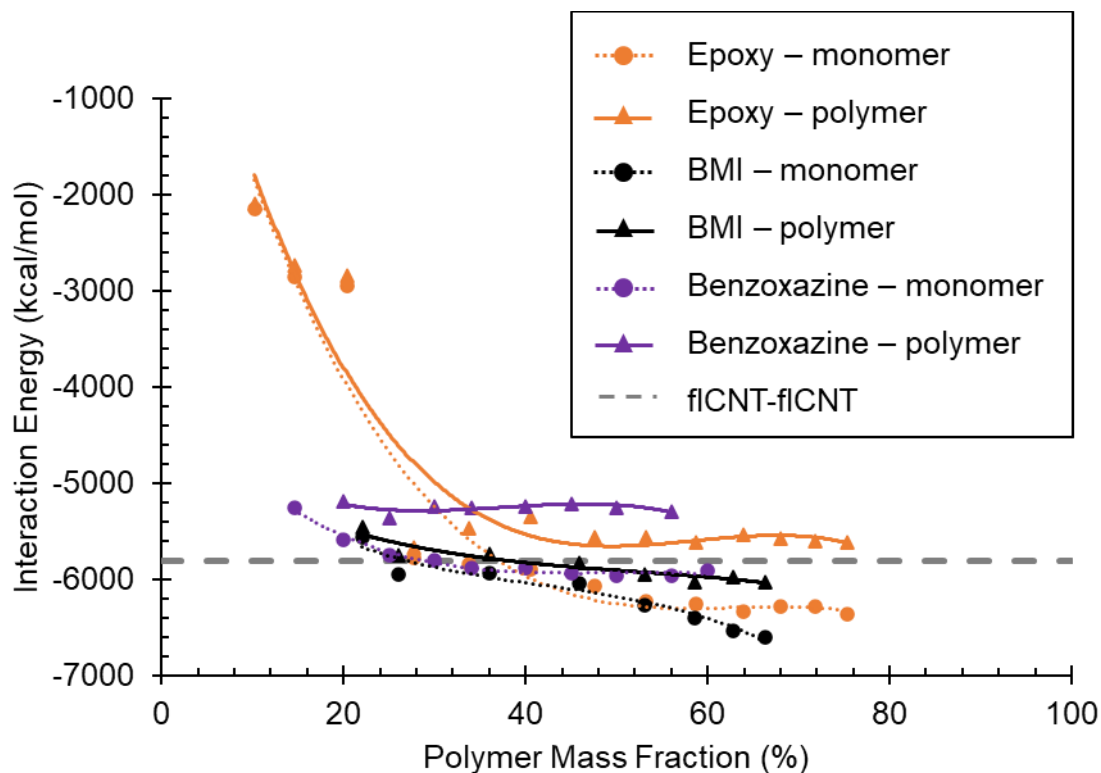


Figure 4. Interaction energy between f1CNTs and polymer layers with varying polymer mass fraction for monomer and polymer cases.

For the epoxy system, the data in Figure 4 indicates the strengthening of interaction depends highly on the effective saturation of the polymer-f1CNT interface. The initial increase is significant and is due to clustering of polymer molecules at the interface for lower mass fractions, which is evident from Figure 3. Well-distributed monomers are observed in the interfacial region at polymer mass fractions 33% or

greater. For higher polymer mass fractions, the fCNTs were completely encompassed by a 10 Å or thicker polymer region, and the interaction energy stays relatively constant.

The data in Figure 4 indicates that the BMI models did not exhibit the same initial steep trend with the interaction energy as observed with the epoxy. However, unlike the epoxy, increases in the interaction energy were observed with increases in the mass fraction over the entire range of mass fractions. This behavior is attributed to the preferential adsorption of the BMPM molecules. The molecular models in this study indicate that BMPM binds better with fCNT than DABPA, which is exemplified in **Error! Reference source not found.** In **Error! Reference source not found.**, the largest fCNT/BMI monomer model, with a monomer mass fraction of 0.66, was divided into equal-width (about 0.7 Å) slices along the Z-direction. The fCNT, BMPM, and DABPA atoms in each slice were counted separately to reveal the molecular spatial variation. The fCNT appears as two sets of double spikes. Note that some waviness in the fCNT caused the peaks to broaden in comparison with perfectly straight layers [45]. The BMPM and DABPA spatial distributions are strikingly contrasting. Immediately flanking the fCNTs are high concentrations of BMPM, but in the same region, the DABPA atoms are depleted. Moving further away from the fCNT layers, the concentration of DABPA increases and becomes more prominent. Essentially, **Error! Reference source not found.** reveals partial monomer separation: the BMPM monomers move toward the fCNT, while the DABPA monomers tend to be driven away from the fCNT. Section S4 from the supporting information provides a more qualitative analysis on BMPM planarization. The epoxy, also a two-part system, did not develop preferential adsorption of either of its components.

From Figure 4, increasing the polymer mass fraction has very little to no effect on the interaction energy of the benzoxazine system. At 34% polymer mass fraction the interaction energy trend converges and remains approximately the same for higher mass fractions. This observation can be explained by **Error!**

Reference source not found., where the lowest mass fraction model displayed perfect separation of the two f1CNT layers. Hence, the interface was completely populated by the polymer atoms for all the mass fractions.

Post-polymerization, the interaction energy plots shift upwards indicating loss of interaction strength due to the new networked polymer topology. For benzoxazine, the effect of polymerization on the interaction energy is significant, however, saturation of the interface for the polymerized system has no effect on the interaction energy. In the case of epoxy and BMI, the interaction energy shifts slightly but maintains the same trend as observed with the unpolymerized models. With BMI, preferential adsorption of BMPM is still present but less impactful. Figure 5 shows the orientation of the phenyl rings in the monomer and polymer structures with respect to the f1CNT surface. It is well-documented that phenyl groups promote aromatic-aromatic non-bonded stacking, a.k.a. π - π stacking [46-49]. The orientations were computed by extracting the dihedral angles of the phenyl rings within the polymer layers. The angle was calculated with respect to the X-Y plane of the f1CNT surface, ignoring deviations caused due to slight waviness as seen in Figure 3. Lower angles represent greater degrees of alignment with the f1CNT surface. The monomer/polymer mass fractions used for this analysis correspond to the converged interaction energies, specifically, BMI: 58.52%, Epoxy: 58.66%, and Benzoxazine: 56%. This analysis was conducted to provide physical insight into the interaction energy trends. Earlier studies have shown the non-bonded interactions between the aromatic groups is a strong contributor towards the interaction energy [49].

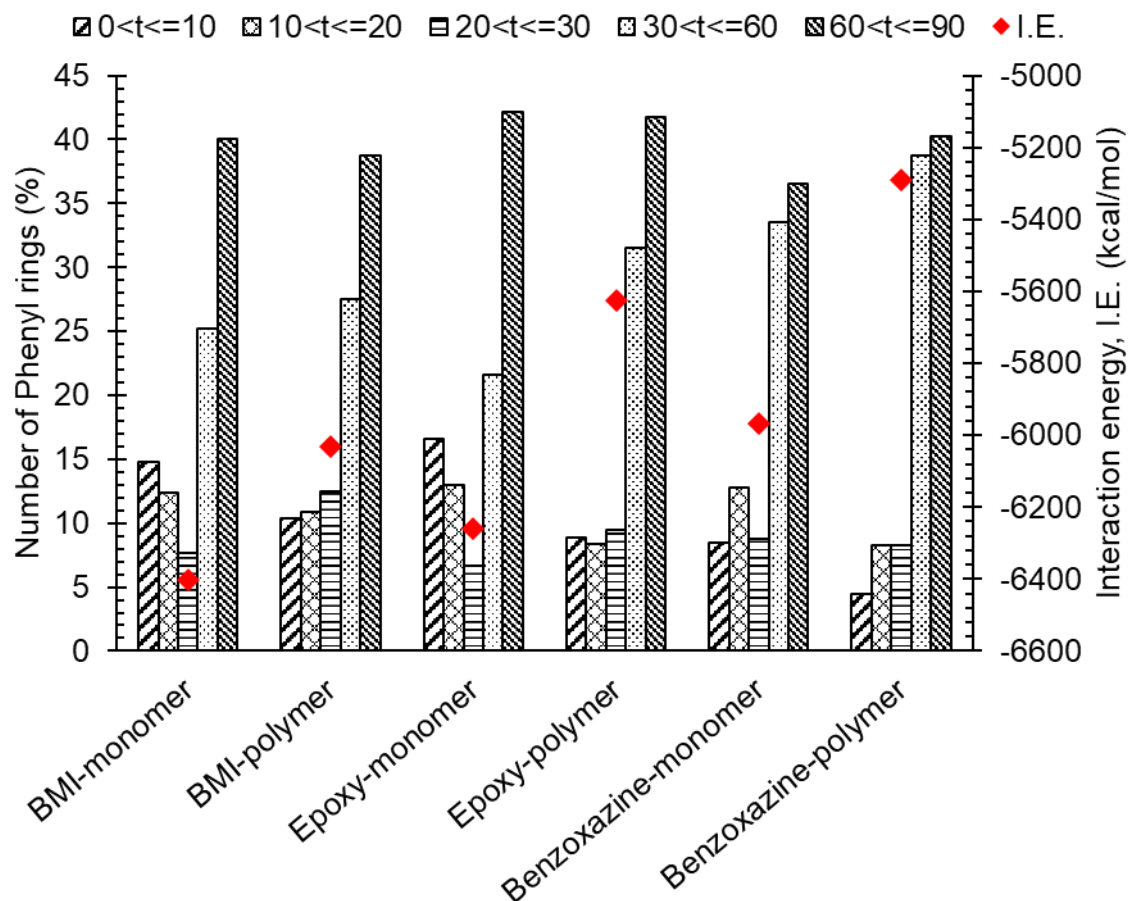


Figure 5. Alignment of phenyl rings (dihedral angles) and interaction energies for BMI, epoxy, and benzoxazine, t (degrees) is dihedral angle formed by the phenyl rings with the XY plane.

Figure 5 clearly shows the decrease in interfacial interaction when the monomers undergo polymerization and result in lower numbers of phenyl rings aligned with the interface. The creation of networks results in additional mobility constraints which results in higher angles between the phenyl rings and the flat aromatic surface. Within each polymer system, the number of phenyl rings with less than 10° angle is reduced after crosslinking. All three resins systems demonstrate similar patterns in interaction energy and polymerization, however, the preferential adsorption in BMI helps in limiting the reduction in interaction energy after polymerization, which is highlighted in Figure 5. The epoxy models show a higher drop in the interaction energy since neither of the two components strongly prefer the f1CNT surface.

Error! Reference source not found. shows the number of phenyl rings with a dihedral angle of less than or equal to 10° with the fCNT surface for the BMI and epoxy systems highlighting the orientations from the individual components. It can be concluded that the BMI models benefit greatly with the increasing mass fractions at the expense of adding mass to the system. Benzoxazine shows poor alignment of the phenyl rings with the surface due to the rigid backbone of the monomer.

Figure 6 shows the interaction energy for multiple polymer systems including those reported in previous studies [11, 12]. The previously studied polymer systems were all single-component systems. The PEEK and non-fluorinated polyimide show the highest degree of interaction, whereas the fluorinated polymers have a relatively low level of interaction because of steric hindrance from the fluorinated groups. The interaction from the benzoxazine is also relatively low. The interaction energy of BMI and epoxy systems lie in the middle of the other polymers. BMI shows slightly better affinity due to the preferential adsorption of BMPM molecules. BMI is the only thermoset in this group with an interaction energy that is lower than that of the bare fCNTs.

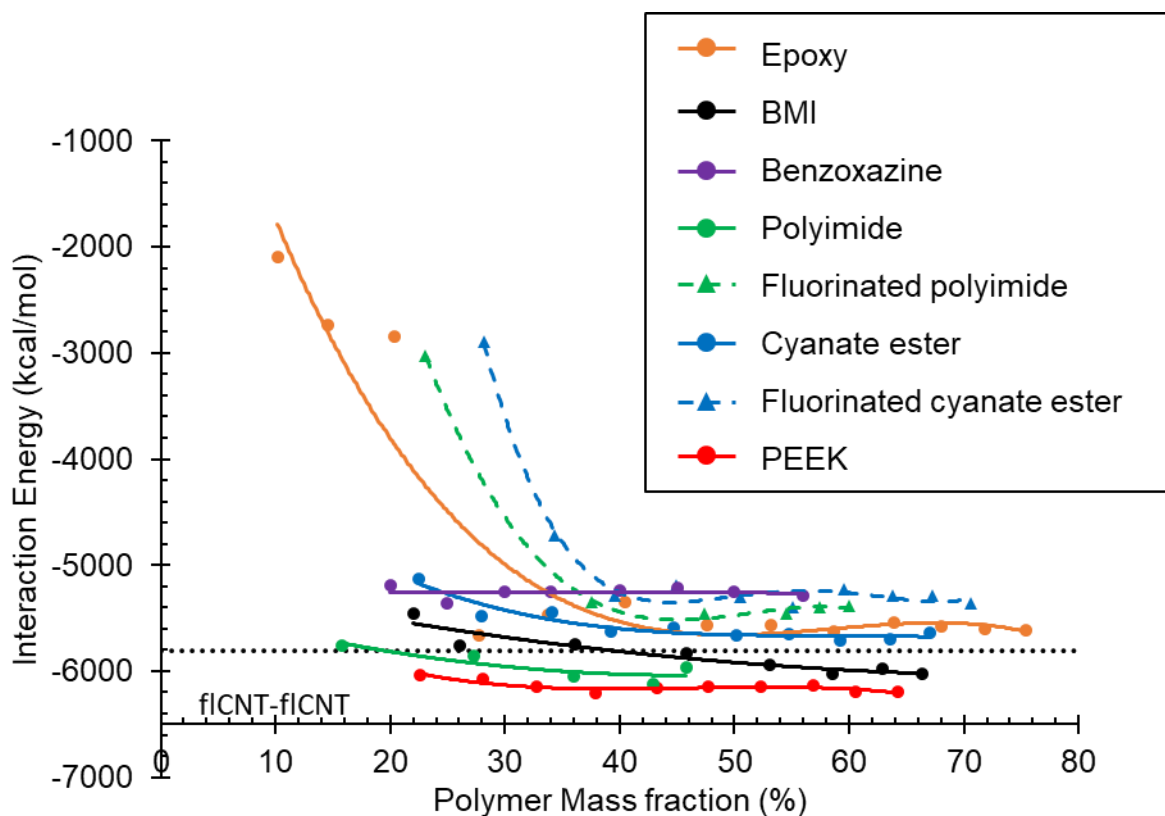


Figure 6. Interaction energy between f1CNTs and polymer layers with varying polymer mass fraction for a wide range of polymers, including data from Pisani et al. [12] and Patil et al. [11].

Frictional Resistance

The results from the friction simulations are detailed in this section for both the monomers and polymers. The trend lines used in all the figures are included to visually distinguish between the datasets and do not hold any physical significance.

Figure 7 reveals the friction force trend for the polymerized and unpolymerized models of all three polymer systems, as well as the friction force associated with f1CNTs with no polymer (commensurate and incommensurate). The incommensurate f1CNT-f1CNT friction case is considered to accurately represent the actual stacking configuration in f1CNT stacks [50, 51]. As reported previously, the presence of a polymer layer results in an increase of two orders of magnitude in the friction force exhibited by the

incommensurate f1CNT-f1CNT [11, 12]. Models with polymer mass fractions of 64% in epoxy, 66% in BMI, and 56% in benzoxazine are used for this comparison. At low velocities, the three polymers (both monomeric and polymeric forms) display a close performance because of the scarcity of polymer atoms at the interface. Benzoxazine displays superior resistance when simulating both low and high velocities. Crosslinking of the model significantly enhances the friction force for BMI and epoxy, but not for the Benzoxazine over most of the range of velocities. The effect of polymerization for these three systems displays an inverse trend as seen from the interaction energy study, where polymerization reduced the interaction, yet increases the frictional force. Polymerization imposes additional restrictions on the movement of the monomeric units by the formation of a polymer network. The formation of a more rigid network causes a greater amount of coarsening (i.e. protrusion of constrained molecular groups into the f1CNT surface) and thus increased interface friction, whereas un-crosslinked monomers can more easily conform to the f1CNT surface and thus form a smoother interface with less friction. Figures S14 and S15 display the minimum and maximum polymer mass fraction models for the three systems for the unpolymerized and polymerized conditions, respectively.

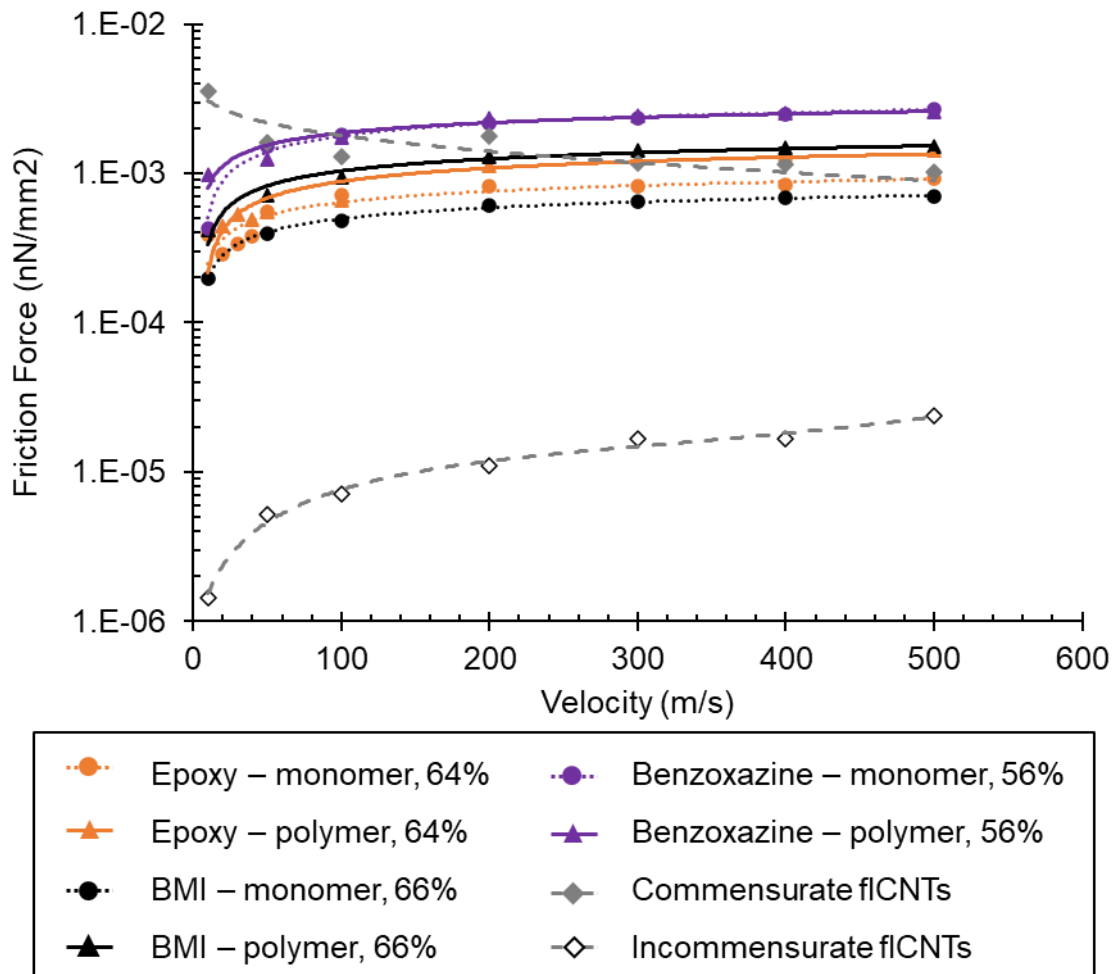


Figure 7. Friction force of the polymer systems and commensurate/incommensurate f1CNTs as a function of velocity for monomer and polymer cases.

In **Error! Reference source not found.**, the effect of polymer mass fraction on the frictional resistance is demonstrated for the entire collection of f1CNT-polymer models and no discernable trend was observed for the range of mass fractions. The results from 10 m/s sliding velocity were chosen for comparison. For all the models, the friction force increases post-polymerization. As seen in Figure 4, the observations indicate an inverse relation between the friction force and interaction energy. That is, polymers exhibiting higher interaction energies exhibited lower frictional resistance, and the systems with lower interaction energy generally displayed better friction force. Also, polymerization degrades the interaction energy of

all the polymers, however, it enhances the friction force for the same systems. Figure S13 from the supporting information shows the data for other velocities and similar trends were observed.

To summarize the results for the friction simulations, Figure 8 shows the frictional force curves of the polymerized models and includes results for the polyimide, PEEK, and cyanate ester systems from Patil et al. [11] and Pisani et al. [12]. The benzoxazine system shows higher frictional resistance in comparison to the fluorinated polymers. It was reported that the fluorinated polymers exhibit higher friction due to the presence of the trifluoromethyl groups [11]. The epoxy and BMI systems also exhibit a good frictional resistance amongst the non-fluorinated polymers. Figure S12 is the supporting information shows the comparison of the same polymers for different polymer mass fractions with a 10 m/s velocity, and like **Error! Reference source not found.**, no discernable trend was observed.

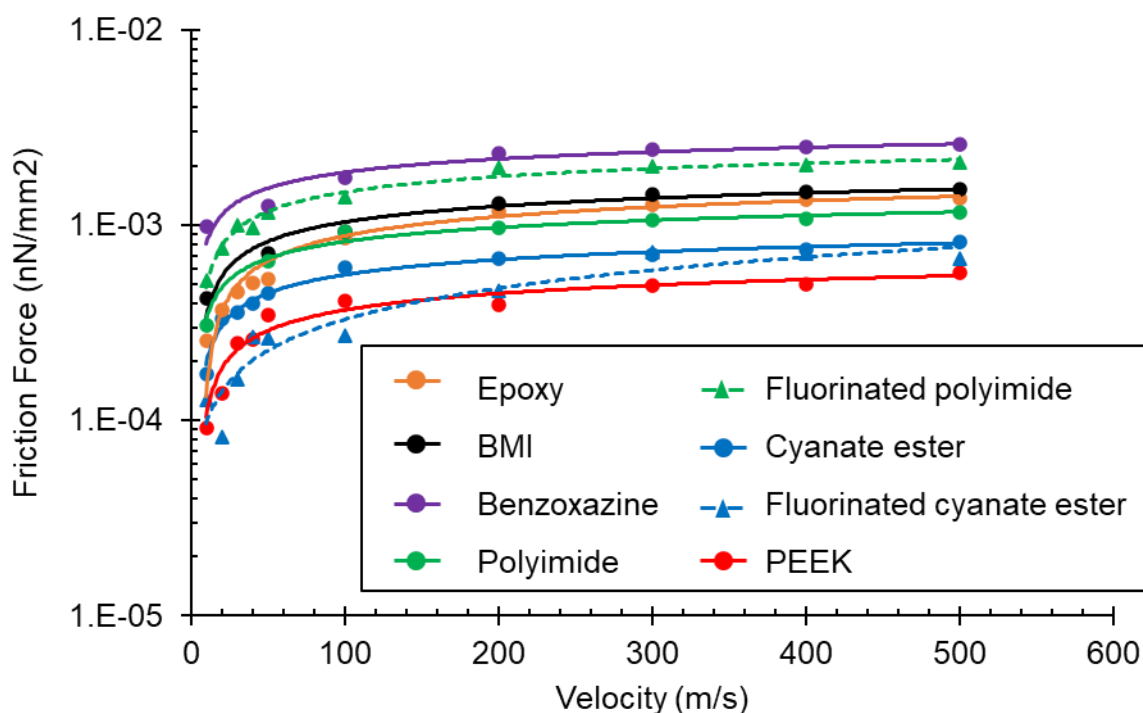


Figure 8. Friction force of polymer systems as a function of velocity for the polymer case, including data from Pisani et al. [12] and Patil et al. [11].

Transverse Strength

Figure 9 shows the stress-strain response from the transverse tension simulations for polymer mass fractions of 41% for epoxy, 36% for BMI, and 34% for benzoxazine. The selection of these polymer mass fractions was based on those of other polymer systems reported in previous work [11, 12]. From the figure, the epoxy and the BMI models exhibit a higher peak strength than the benzoxazine. However, the benzoxazine system displays a higher toughness which is evident from the corresponding curve not converging to the 0 MPa stress value. It is important to note that stress-strain data that is generated using all-atom MD simulations inherently includes a strain rate effect that results from the simulated deformation rates that are orders of magnitude above laboratory-observed deformation rates [24, 52, 53]. Thus, the stress strain response shown in the figure is not necessarily what would be expected from an experimental tensile test of the interfacial region. However, the relevant information from the figure is the comparative response of the different systems. MD-generated stress-strain curves provide a quantitative comparison the response of different systems to discern trends and physical insight. **Error! Reference source not found.** shows snapshots of the three models either at the end of simulation or when one of the polymer layers completely separated.

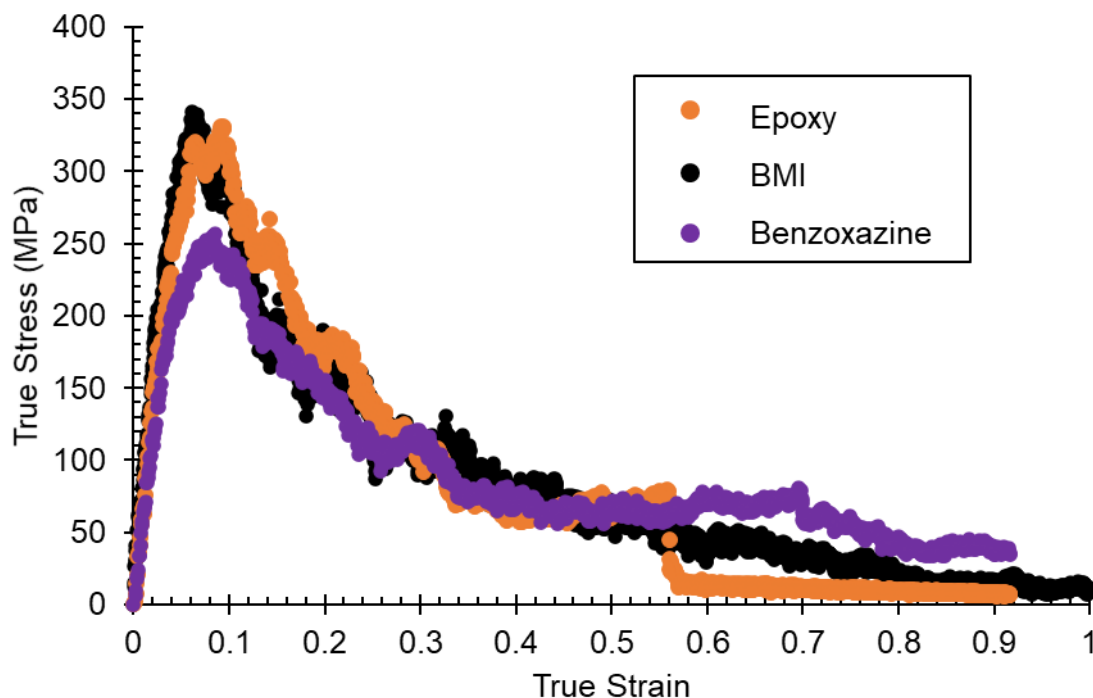


Figure 9. Stress-strain curves of the three polymerized systems in transverse tension.

Figure 10 includes the transverse tension results for all the polymer systems including the corresponding data for the polyimide, cyanate ester, and PEEK systems from previous studies [11, 12]. The stiffness, toughness, and peak strength values are normalized with respect to the results obtained from a neat f1CNT-f1CNT transverse tension simulation. From the comparison, BMI shows the best performance in all the three metrics. Epoxy shows the second highest stiffness and peak strength but lower toughness than benzoxazine and the fluorinated cyanate ester. From **Error! Reference source not found.**, it is clear that separation of the polymer layer occurs much earlier in the epoxy system relative to the BMI and benzoxazine systems, resulting in the lower overall toughness.

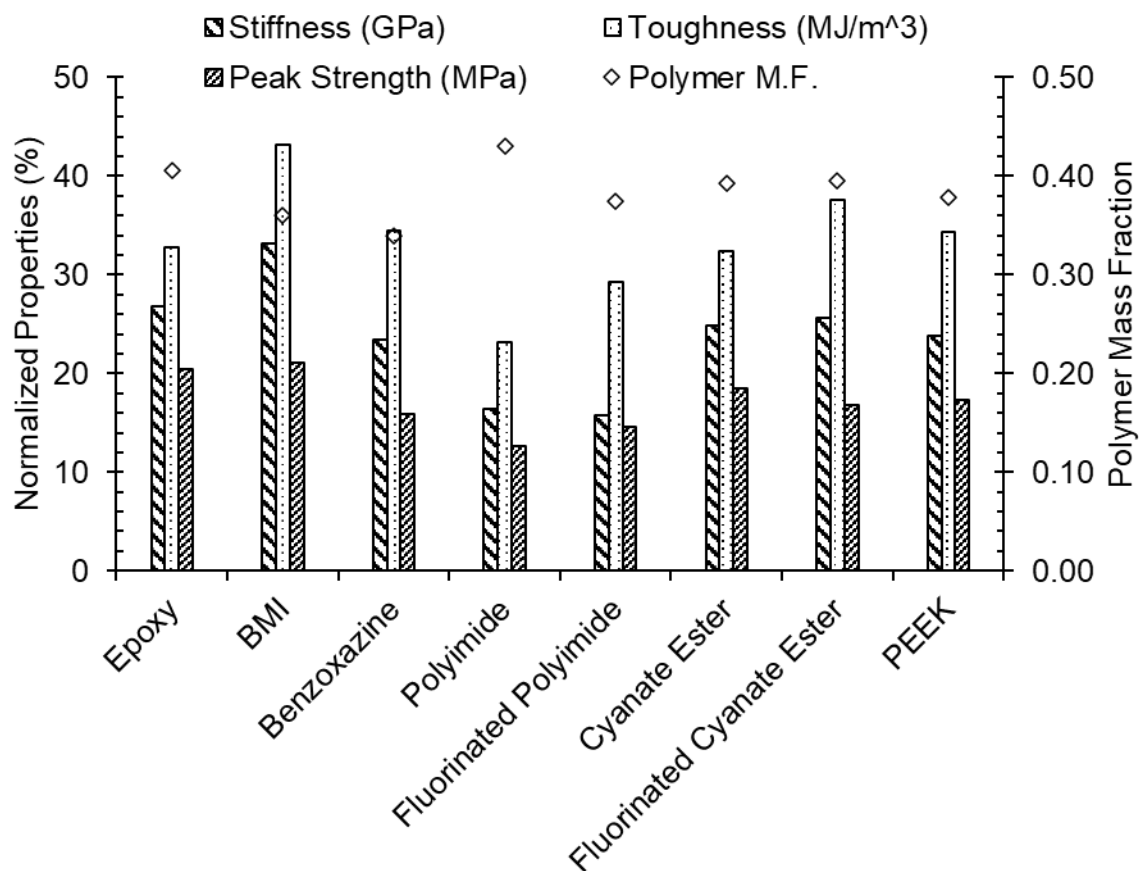


Figure 10. Normalized stiffness, toughness, and peak strength, and the corresponding polymer mass fraction for the polymerized polymer/fCNTs.

Conclusion

BMI produces the best overall compatibility with the fCNTs with the epoxy showing a similar trend but with a slight under-performance. Including the previously reported systems, PEEK still shows the best interaction with the fCNTs with the polyimide and BMI also showing higher interaction than bare fCNTs [11, 12]. However, benzoxazine exhibits a much superior friction force than the other two systems in this study and the two fluorinated systems from Patil et al. [11] and Pisani et al. [12]. With a best performance in two out of the three metrics, including the three sub-metrics from transverse tension, the BMI appears to be the polymer matrix of choice when considering the fCNT stacks. However, in the design of such

nanocomposites, careful consideration may be required in balancing the three described metrics as per the application. Therefore, the molecular insights gained from this research can be helpful in guiding the selection of resin systems for the engineering of new f1CNT-based composites. The results of this study are not generally applicable to traditional carbon fiber/polymer composites, as carbon fiber generally has a significant sizing layer on the fiber surface, and carbon fibers generally don't have the pristine aromatic surface that was studied herein for f1CNTs.

Supporting Information

The following document is available free of charge. The document (PDF) includes details on the polymerization for the three resin systems, configuration of all the nanocomposite models, qualitative analysis on BMPM planarization and additional details on the frictional resistance results.

Acknowledgements

This research was supported by the NASA Space Technology Research Institute (STRI) for Ultra-Strong Composites by Computational Design (US-COMP), grant NNX17AJ32G. SUPERIOR, a high-performance computing cluster at Michigan Technological University, was used in obtaining the MD simulation results presented in this publication.

References

1. NASA, *2020 NASA Technology Taxonomy*. 2020, NASA.
2. Kim, J.-W., et al., *Assessment of carbon nanotube yarns as reinforcement for composite overwrapped pressure vessels*. Composites Part A: Applied Science and Manufacturing, 2016. **84**: p. 256-265.
3. Kim, J.-W., et al., *Modifying carbon nanotube fibers: A study relating apparent interfacial shear strength and failure mode*. Carbon, 2021. **173**: p. 857-869.
4. Bellucci, S., et al., *CNT composites for aerospace applications*. Journal of Experimental Nanoscience, 2007. **2**(3): p. 193-206.

5. Baur, J. and E. Silverman, *Challenges and Opportunities in Multifunctional Nanocomposite Structures for Aerospace Applications*. MRS Bulletin, 2007. **32**(4): p. 328-334.
6. Siochi, E.J. and J.S. Harrison, *Structural nanocomposites for aerospace applications*. MRS Bulletin, 2015. **40**(10): p. 829-835.
7. Downes, R.D., et al., *Geometrically constrained self-assembly and crystal packing of flattened and aligned carbon nanotubes*. Carbon, 2015. **93**: p. 953-966.
8. Jolowsky, C., et al., *Microstructure evolution and self-assembling of CNT networks during mechanical stretching and mechanical properties of highly aligned CNT composites*. Composites Science and Technology, 2018. **166**: p. 125-130.
9. Chen, J., et al., *Interfacial characteristics of carbon nanotube-polymer composites: A review*. Composites Part A: Applied Science and Manufacturing, 2018. **114**: p. 149-169.
10. Desai, A.V. and M.A. Haque, *Mechanics of the interface for carbon nanotube-polymer composites*. Thin-Walled Structures, 2005. **43**(11): p. 1787-1803.
11. Patil, S.U., et al., *Interfacial characteristics between flattened CNT stacks and polyimides: A molecular dynamics study*. Computational Materials Science, 2020. **185**.
12. Pisani, W.A., et al., *Interfacial modeling of flattened CNT composites with cyanate ester and PEEK polymers*. Composites Part B: Engineering, 2021. **211**.
13. Song, Y., et al., *Carbon nanotube sensor thread for distributed strain and damage monitoring on IM7/977-3 composites*. Smart Materials and Structures, 2014. **23**(7).
14. Kaiser, A.L., I.V. Albelo, and B.L. Wardle, *Fabrication of Aerospace-grade Epoxy and Bismaleimide Matrix Nanocomposites with High Density Aligned Carbon Nanotube Reinforcement*, in *AIAA Scitech 2020 Forum*. 2020, American Institute of Aeronautics and Astronautics.
15. Liu, Y., et al., *Shape memory polymers and their composites in aerospace applications: a review*. Smart Materials and Structures, 2014. **23**(2).
16. Adrian Lowe, B.F., Vincent Otieno-Alego, *Interfacial ageing of high temperature carbon/bismaleimide composites*. Composites Science and Technology, 2002. **33**(10): p. 1289-1292.
17. Gu, A., et al., *Bismaleimide/carbon nanotube hybrids for potential aerospace application: I. Static and dynamic mechanical properties*. Polymers for Advanced Technologies, 2007. **18**(10): p. 835-840.
18. Kirmani, M.H., et al., *Cure Behavior Changes and Compression of Carbon Nanotubes in Aerospace Grade Bismaleimide-Carbon Nanotube Sheet Nanocomposites*. ACS Applied Nano Materials, 2021.
19. Hatsuo Ishida, T.A., *Handbook of Benzoxazine Resins*. 2011: Elsevier.
20. Comer, A.J., et al., *OOA (Out-of-Autoclave) manufacturing of benzoxazine resin-systems by lri (liquid-resin-infusion) for ambient and high temperature aerospace applications*. 2014.
21. Barile, C., C. Casavola, and F. De Cillis, *Mechanical comparison of new composite materials for aerospace applications*. Composites Part B: Engineering, 2019. **162**: p. 122-128.
22. Bandyopadhyay, A., et al., *Molecular modeling of crosslinked epoxy polymers: The effect of crosslink density on thermomechanical properties*. Polymer, 2011. **52**(11): p. 2445-2452.
23. Pisani, W.A., et al., *Multiscale modeling of PEEK using reactive molecular dynamics modeling and micromechanics*. Polymer, 2019. **163**: p. 96-105.
24. Radue, M.S., et al., *Comparing the Mechanical Response of Di-, Tri-, and Tetra-functional Resin Epoxies with Reactive Molecular Dynamics*. J Polym Sci B Polym Phys, 2018. **56**(3): p. 255-264.

25. Plimpton, S., *Fast Parallel Algorithms for Short-Range Molecular Dynamics*. Journal of Computational Physics, 1995. **117**: p. 1-19.
26. Heinz, H., et al., *Thermodynamically consistent force fields for the assembly of inorganic, organic, and biological nanostructures: the INTERFACE force field*. Langmuir, 2013. **29**(6): p. 1754-65.
27. Pramanik, C., et al., *Carbon Nanotube Dispersion in Solvents and Polymer Solutions: Mechanisms, Assembly, and Preferences*. ACS Nano, 2017. **11**(12): p. 12805-12816.
28. Dharmawardhana, C.C., et al., *Reliable computational design of biological-inorganic materials to the large nanometer scale using Interface-FF*. Molecular Simulation, 2017. **43**(13-16): p. 1394-1405.
29. Hundley, J.M., et al., *Multi-Scale Modeling of Metal-Composite Interfaces in Titanium-Graphite Fiber Metal Laminates Part I: Molecular Scale*. Open Journal of Composite Materials, 2011. **01**(01): p. 19-37.
30. Radue, M.S., et al., *Molecular Modeling of Cross-Linked Polymers with Complex Cure Pathways: A Case Study of Bismaleimide Resins*. Macromolecules, 2018. **51**(5): p. 1830-1840.
31. ALLEN, H.I.a.D.J., *Physical and Mechanical Characterization of Near-Zero Shrinkage Polybenzoxazines*. Journal of Polymer Science: Part B: Polymer Physics, 1996. **34**: p. 1019-1030.
32. Zhe Liu, Y.-S.D., Matthew Lundblad, Ayou Hao and Zhiyong Liang, Youssef Aider and Yeqing Wang, *Lightweight and Flexible Thermal Protection Systems for High Temperature Composite Applications*, in SAMPE 2020. 2020: Virtual Series.
33. Cheng, Q., et al., *High Mechanical Performance Composite Conductor: Multi-Walled Carbon Nanotube Sheet/Bismaleimide Nanocomposites*. Advanced Functional Materials, 2009. **19**(20): p. 3219-3225.
34. Cheng, Q., et al., *Functionalized carbon-nanotube sheet/bismaleimide nanocomposites: mechanical and electrical performance beyond carbon-fiber composites*. Small, 2010. **6**(6): p. 763-7.
35. Sandi G. Miller, J.K.S., Daniel A. Scheiman, Michael Maryanski, and Michelle Schlea, *STUDY OF OUT-TIME ON THE PROCESSING AND PROPERTIES OF IM7/977-3 COMPOSITES*, in SAMPE 2010. 2010: Seattle, WA.
36. Vincent J.Lopata, C.B.S., Ajit Singh, Christopher J.Janke, George E.Wrenn, Stephen J.Havens, *Electron-beam-curable epoxy resins for the manufacture of high-performance composites*. Radiation Physics and Chemistry, 1999. **56**(4): p. 405-415.
37. Ishida, Y.-X.W.a.H., *Synthesis and Properties of New Thermoplastic Polymers from Substituted 3,4-Dihydro-2H-1,3-benzoxazines*. Macromolecules, 2000. **33**(8): p. 2839-2847.
38. Okabe, T., et al., *Curing reaction of epoxy resin composed of mixed base resin and curing agent: Experiments and molecular simulation*. Polymer, 2013. **54**(17): p. 4660-4668.
39. Saiev, S., et al., *Modeling the formation and thermomechanical properties of polybenzoxazine thermosets*. Polymer Chemistry, 2017. **8**(38): p. 5988-5999.
40. Thompson, S., et al., *Exploring Structure(-)Property Relationships in Aromatic Polybenzoxazines Through Molecular Simulation*. Polymers (Basel), 2018. **10**(11).
41. Won-Kook Kim, W.L.M., *A fully atomistic model of an amorphous polybenzoxazine at bulk density*. Computational and Theoretical Polymer Science, 1998. **8**: p. 353-361.
42. Damirchi, B., et al., *ReaxFF Reactive Force Field Study of Polymerization of a Polymer Matrix in a Carbon Nanotube-Composite System*. The Journal of Physical Chemistry C, 2020. **124**(37): p. 20488-20497.

43. Bogusz, S., T.E. Cheatham, and B.R. Brooks, *Removal of pressure and free energy artifacts in charged periodic systems via net charge corrections to the Ewald potential*. The Journal of Chemical Physics, 1998. **108**(17): p. 7070-7084.
44. Radue, M., *Molecular Modeling of Aerospace Polymer Matrices Including Carbon Nanotube-Enhanced Epoxy*, in *Mechanical Engineering-Engineering Mechanics*. 2017, Michigan Technological University. p. 126.
45. Al Mahmud, H., et al., *Multiscale modeling of carbon fiber- graphene nanoplatelet-epoxy hybrid composites using a reactive force field*. Composites Part B: Engineering, 2019. **172**: p. 628-635.
46. Huber, R.G., et al., *Heteroaromatic pi-stacking energy landscapes*. J Chem Inf Model, 2014. **54**(5): p. 1371-9.
47. McGaughey, G.B., M. Gagne, and A.K. Rappe, *pi-Stacking interactions. Alive and well in proteins*. J Biol Chem, 1998. **273**(25): p. 15458-63.
48. Mutasem Omar Sinnokrot, E.F.V., and C. David Sherrill, *Estimates of the Ab Initio Limit for $\pi-\pi$ Interactions: The Benzene Dimer*. J. Am. Chem. Soc., 2002. **124**(36): p. 10887-10893.
49. Mingjun Yang, V.K., and Michael Zaiser, *Interactions between Polymers and Carbon Nanotubes: A Molecular Dynamics Study*. J. Phys. Chem. B, 2005. **109**(20): p. 10009-10014.
50. Xu, H., J. Al-Ghalith, and T. Dumitrică, *Smooth sliding and superlubricity in the nanofriction of collapsed carbon nanotubes*. Carbon, 2018. **134**: p. 531-535.
51. Xu, H., et al., *Collapsed carbon nanotubes: From nano to mesoscale via density functional theory-based tight-binding objective molecular modeling*. Carbon, 2019. **143**: p. 786-792.
52. G. M. Odegard, S.U.P., P. Deshpande, K. Kanhaiya, J. Winetrout, H. Heinz, S. Shah, M. Maiaru, *Molecular Dynamics Modeling of Epoxy Resins using the Reactive Interface Force Field*. 2021: arXiv:2107.14286 [cond-mat.mtrl-sci].
53. Odegard, G.M., et al., *Predicting mechanical response of crosslinked epoxy using ReaxFF*. Chemical Physics Letters, 2014. **591**: p. 175-178.